Hindawi
Advances in Civil Engineering
Volume 2019, Article ID 7581061, 18 pages
https://doi.org/10.1155/2019/7581061

Research Article

Mechanical Properties of Bump-Prone Coal with Different Porosities and Its Acoustic Emission-Charge Induction Characteristics under Uniaxial Compression

Xin Ding,[1] Xiaochun Xiao,[1,2] Xiangfeng Lv,[3] Di Wu,[1] and Jun Xu[2]

[1]*State Key Laboratory of Coal Mine Disaster Dynamics and Control, Chongqing University, Chongqing 400044, China*
[2]*Key Laboratory of Rock Mechanics and Geohazards of Zhejiang Province, Shaoxing University, Shaoxing, Zhejiang 312000, China*
[3]*School of Civil and Resource Engineering, University of Science & Technology Beijing, Beijing 100083, China*

Correspondence should be addressed to Xiaochun Xiao; xxc7902@163.com; Xiangfeng Lv; lvxiangfeng2006@126.com; and Jun Xu; jxu1120@126.com

Received 31 March 2019; Revised 5 May 2019; Accepted 9 May 2019; Published 2 June 2019

Academic Editor: Cumaraswamy Vipulanandan

Discreteness of mechanical property affected by the intimal damage, which emerged with various degrees of material composition and geological structure, is the difference in porosity macroscopically. Although various porosities directly affect fracture activity, damage evolution and mechanical behaviour of coal bring on the bump-prone assessment error, and disaster happened "ahead of time" in deep underground energy source exploration, little research to date has focused on them. In this paper, the mechanical properties of bump-prone coal samples with different porosities were studied by uniaxial compression test and the initial damage caused by gangue and organic fracture in coal observed by CT. The result indicated that the evolution of coal strength and the logarithm of porosity were expressed by a linear negative correlation and the elastic modules decreased with the initial damage increased. A new quantitative description of damage variables is established by theoretical derivation to reflect the process of cracks formation and expiation in coal, based on volumetric strain and initial porosity. According to the Mohr–Coulomb principle, the effective stress of coal sample with higher the porosity is more likely to reach the shear strength and destruction. The amplitudes and accumulation of AE energy and charge pulse indeed vary with the stress loading stages and strength. The frequency of AE waveform is dominated in three bands (1~50 kHz, 100~150 kHz, and 175~200 kHz) and that of charge induction had one frequency band 1~100 Hz, and the amplitudes of time domain and main frequency components increased with stress improved. Both of them originated from cracks and belong to homologous signals, crack development bound to be accompanied by stress wavelet, not necessarily free charge; meanwhile, charge pulse being emerged means there must be cracks interaction and the acoustic emission signals are generated prior to charge induction.

1. Introduction

Coal is a strong nonlinear engineering rock [1], in which the structure of pores and cracks is naturally widespread [2], prone to instability and induced coal bump hazard [3]. To date, improving the accuracy of the dynamic disaster risk assessment and forming an effective and reliable monitoring method is always an engineering challenge that urgently needs to be solved for the coal production industry of China and the world, predominantly for the purpose of disaster prevention and control.

During underground mining, the mechanical properties of coal are related to the fracture development. Therefore, it is important to sample for the difference in any study of strength to determine predictive initial porosity, and it also relates to damage evolution and bump-proneness, which are useful factors for coal bump risk assessment of stope coal mass and eliminating the discrete mechanical behaviour of coal. van Krevelen [4] investigated the evolution of the mechanical properties of coal with different lithotypes (organic compositions), rank (thermal maturity), and grade (mineral matter content), and the relationships between

these parameters on the basis of many experiments indicated that these factors were influences directly for coal drillability, fracture stimulation, breakage, and grindability. Pattinson et al. [5], and Zhao et al. [6] discussed the variation of the stress field caused by geological structure with the initial fracture and permeability of coal by field monitoring and laboratory testing and reported that the fractures have a significant influence on the distribution of mining stress zones and the bearing structure of the coal mass. With the development of CT technology, the incomparable advantages in nondestructive detection of rocks and real-time detection of cracks under different conditions have become more obvious. Then, more and more rock mechanics experiments have introduced the exploration of the damage characteristics of samples. Relevant studies have been carried out by Ray et al. [7], Konecny and Kozusnikova [8], Mao et al. [9], and Cai et al. [10]. The results show that the cracks in coal can be observed by CT scan, and the variation of porosity reflects the opening and closing cracks. Cracks develop gradually in the later elastic stage. There was obvious development of macrocracks in the strengthening and postpeak stages, which formed and expanded along the original defects. The degree of fracture development directly affects the characterization of the mechanical behaviour of coal. Klawitter et al. [11] showed that the mechanical behaviour relates to rank and can control fracture as well as breakage behaviour of a given coal. The original cracks play an important role in the elastic-plastic evolution of coal failure. However, to date, the exact mechanical evolution causing coal mass structure failure and instantaneous instability for a coal bump is still unresolved. The existing research focusses on the coal properties influenced by fracture but shows little focus on definite description and the mechanism between porosity and strength. How we can use the measured parameters to reflect the dynamic evolution of coal damage remains a key concern for coal mass failure determination. Multiple monitoring method approaches can help us to obtain precursory information with regard to cracks and damage, but the work of effective information acquisition and inversion is not easy for us.

It has been widely confirmed that [12–14] there were sound and electrical anomalies during the coal or rock failure process. Many scholars have carried out extensive related research on this phenomenon. Rudajev et al. [15] found that the variation and values of autocorrelation coefficients incorporate significant information about the stress state and about the stage of rock disintegration. The spatial foci distribution also contains a wealth of information. Shkuratnik et al. [16] and Lavrov and Shkuratnik [17] observed that the AE phenomenon was affected by the parameters and space-time dynamics of the geological material structure in samples. Su et al. [18] discussed the application of acoustic emission (AE) analysis for the evaluation of distinctly designed UCG models. The AE analysis revealed that AE activity is closely related to the crack initiation and extension. He et al. [19] carried out single-face dynamic unloading tests under true-triaxial conditions for limestone samples, pointing out that the frequency amplitude of AE signals varies with coal bump stages. Yang et al. [20] reported that the external stress condition has a transition effect on the AE event energy distribution and AE activity pattern. Kuksenko et al. [21] found that the relaxation of the polarization is identical in nature for both cases and is basically a thermally activated process. They estimated the activation energy for motion of charge carriers leading to the relaxation of these fields. Freund et al. [22] reported newly discovered dual outflow currents from stressed igneous rocks and their magnitudes for low-frequency electromagnetic (EM) emissions based on a laboratory experiment. Lv et al. [23] found that the slip, dislocations, and inhomogeneous deformations of the crack interface and lattice cause charge breakthrough and established a theoretical model of microcrack slip friction charge. Yamada et al. [24], Rabinovitch [25], Eccles et al. [26], Zhao and Jiang [27], Xiao et al. [28], Archer et al. [29], and Pasiou and Triantis [30] discussed the similarities and differences in signals generated in coal or rock failure such as acoustic emission, charge induction, infrared radiation temperature (AIRT), strain, and electromagnetic radiation (EMR), which were based on laboratory experiments, showing that both of them inverted the loading state of coal or rock with a good sensitivity to crack generation and development. The strain and AIRT have a single signal parameter but multiple AEs, charge inductions, and EMRs from the time and frequency domain. In addition, the compound signal of binary or multivariate monitoring methods reduced information omissions effectively and has represented underground dynamic disaster early warning research in a new development direction. However, previous studies about acoustic emission of coal failure still focused mainly on the time domain signal because its spectral characteristics are less involved, and the situation is the same in charge induction. To date, the exact mechanism did not form a consensus, and the evolution of the tow method for the samples with significant discrete mechanical properties is still unclear. These are the basis of the compound signals in the early warning method, which is based on acoustic emission and charge induction and needs to be solved.

In this study, the entire deformation process of bump-prone coal samples with different porosities taken from the Wulong Mine of the Fuxin Coal Group in China under uniaxial loading has been investigated by using the acoustic emission and charge induction methods simultaneously and continuously in real time. The initial damage in the coal samples with different porosities obtained by CT scan and the relationship between strength and porosity were calculated. A new quantitative description of the damage variables based on volumetric strain and initial porosity was established by theoretical derivation, and the mechanism of coal failure was discussed. The time-frequency domain characteristics of acoustic emission and charge induction during coal failure were discussed. The results provide a reliable theoretical and experimental basis for obtaining precursor information to monitor coal bumps.

2. Materials and Methods

2.1. Preparation of Specimens. The coal specimens in the test were originally from a depth of 800 m in the Wulong Mine,

which is a long-flaming coal. The Wulong Mine is located in the middle of the Fuxin Coal Group in the northeast of China, as shown in Figure 1. The Wulong Mine covers an area of 11.76 km^2 and has a monoclinic structure, strike N35°~78°E, lean SE12°~55°, dip angle 5°~24°, average 12°. There were 7 faults in the mine field. Since the mine was built, there have been more than 20 recorded cases of coal bump accidents with a high magnitude and a large degree of damage and casualties. The Wulong Mine is a typical coal bump mine, and a scene of a coal bump accident is shown in Figure 2.

Due to the influence of both structure and primary components in the mine field, the soft inclusion gangue in the coal sample was obvious. The main component of the soft gangue was the high porosity of the carbon and mica. The bulk density of the cores ranges from 1291 to 1439 kg/m^3. Samples collected from the target coal seam were sent to the laboratory. Cylindrical specimens measuring Φ50 mm × 100 mm were prepared, and both ends of each specimen were polished to ensure that the flatness error was less than ±0.02 mm (Figure 3).

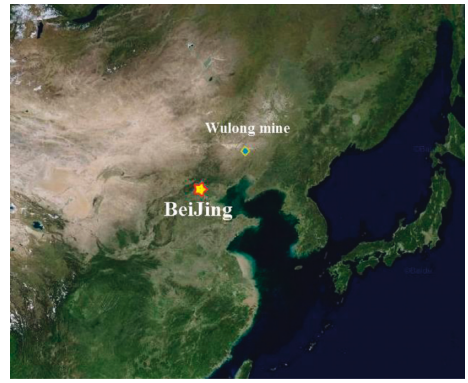

Figure 1: Location map of the Wulong mine of the Fuxin Coal Group.

Figure 2: Situation of coal bump disaster that occurred in a roadway.

2.2. Experimental Setup and Scheme. Tests were conducted at the Liaoning Key Laboratory of Mine Environment and Disaster Mechanics, Liaoning Technical University, Fuxin city. A TAW-2000 digital hydraulic servo test machine was used for the uniaxial compression test, and load and displacement data acquisition processes were used to obtain the measurements automatically, which made by Jinli Test Techology Co., Ltd, Jilin province, P. R. China. The machine had a compression capacity of 2000 kN with a resolution of the number of impressions at 5‰, as shown in Figure 4(a).

A USEA-2 AE monitoring system, manufactured by Beijing Sound Technology, Ltd., was used in this study. This monitoring system was composed of AE transducers, a preamplifier, signal acquisition, and processing and recording units. The AE transducers were placed on the surface of the coal, and the coupling surface was coated with a coupling agent. The sensor frequency was 10~1000 kHz, and its sensitivity peak was >75 dB. The sampling frequency was set to 1000 kHz, the parameters and waveform threshold values were 40 dB, the main playback gain was 20 dB, and the sampling point was 1024.

A noncontact charge signal monitoring system was developed specifically for laboratory experiment; it included a microelectro-sensitive alloy sheet, a preamplifier, an acquisition instrument, and a computer. The basic working principle of the system is the self-potential anomaly of coal or rock mass caused by free charge, which forms a microelectric field around the sample, resulting in the directional movement of the positive and negative charge inside the alloy sheet in a short time under the effect of charge induction. The charge can induce transiently weak current, and this process lasts until the electric field disappears because of reduction of the free charge in the coal or rock. Therefore, the alloy sheet restores static balance. The basic sketch of charge preamplifier is shown in Figure 4(b), and a standard capacitive component is used to amplify and convert the transient weak current generated by the alloy sheet electric induction into a voltage signal output, the A/D conversion by digital signal acquisition instrument, and acquisition and storage. During the experiment, the charge preamplifier was mounted on the cylinder. The alloy sheet had no contact with the coal surface, and we ensured that the distance between them was maintained at 5 mm in each experiment, as shown in Figure 4(a), where the sensor frequency was 1~1000 Hz and the sensitivity peak >75 dB. The conversion ratio between charge input and analogue output is 1 pc/10000 mV. The sampling frequency was set to 1000 Hz, and the sampling point was 1024.

2.3. Experimental Scheme. The experiment involved a uniaxial compression test of coal, where the loading rate was set at 0.01 mm/s and the following procedure was carried out:

(1) Place the coal specimen between the top and bottom indenters at each coupling surface with an insulating pad to prevent charge overflow, as shown in Figure 4(c). Debug equipment and set parameters.

(2) Start the mechanical system, AE monitoring system, charge induction signal monitoring system, and deformation monitoring system simultaneously to collect information during the coal deformation and failure process. Convert the analogue signal into a digital signal for storage based on the A/D conversion. Increase stress using the digital hydraulic servo test machine until the final destruction of the coal.

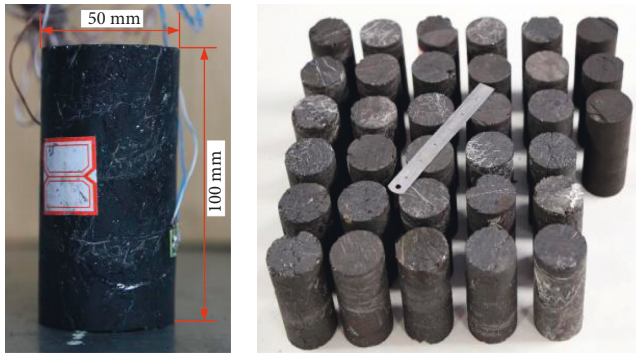

(a) (b)

Figure 3: Coal specimens.

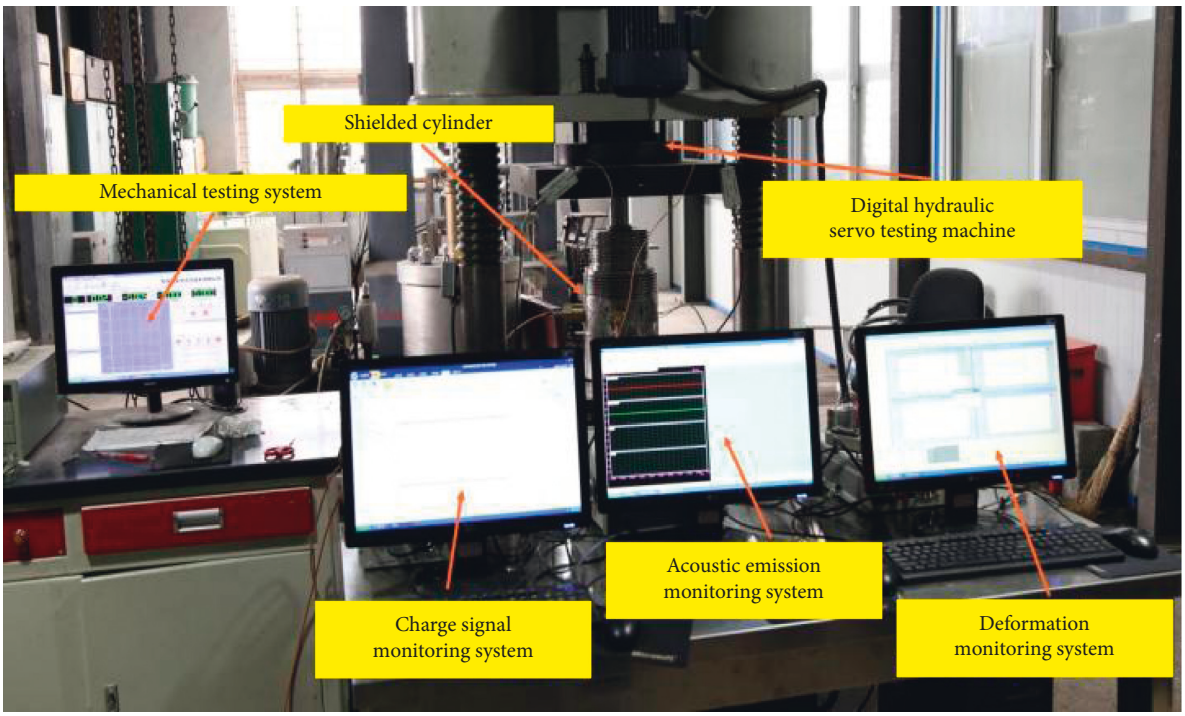

(a)

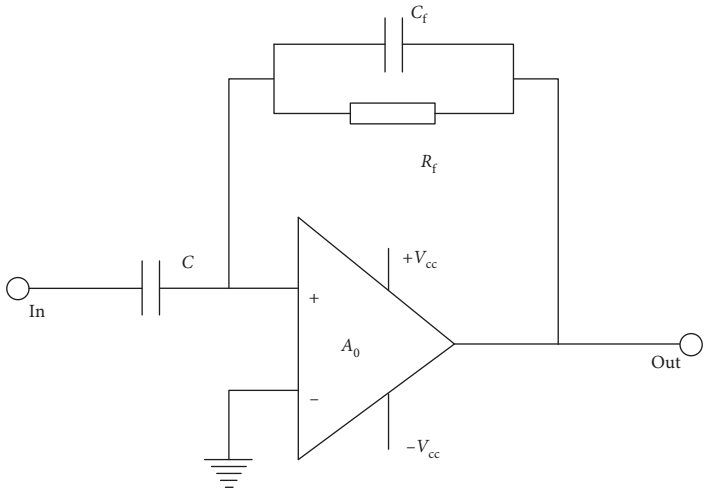

(b)

Figure 4: Continued.

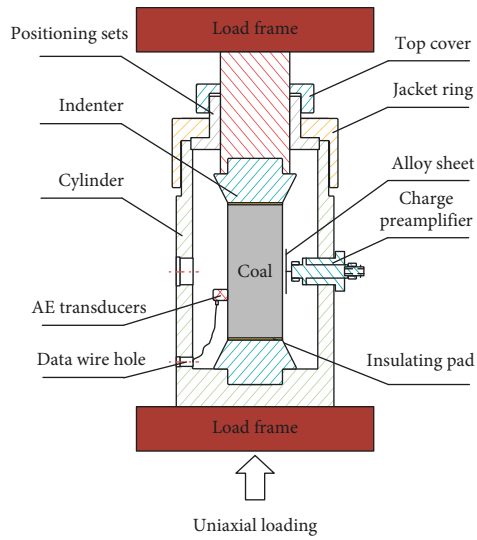

(c)

Figure 4: System for testing. (a) Instruments of the testing system. (b) Basic sketch of charge preamplifier. (c) Structural diagram of the shield cylinder. The location of the AE transducers and charge preamplifier is shown, but the number of sensors is not limited.

(3) Store the result. Screen the fragments of coal and take photos and carry out postprocessing of the data on a PC based on MATLAB, Origin, or similar software.

3. Experimental Result of Coal Failure and Discussion

3.1. Mechanical Properties of Bump-Prone Coal with Different Porosities. Shown in Figure 5 are three typical stress-strain curves of coal that failed under simple compression, which were affected by gangue and fracture. The results show that the stress-strain relationship in the process of loading was still divided into four stages of compaction, elasticity, strengthening, and a postpeak phase, even though there were some differences in fracture and gangue content. From the surface of the coal, as the fracture and gangue content gradually decreased, the elastic phase of the curve grew. The average modulus of elasticity and strength increased significantly, and the stress drop phenomenon is obvious at the postpeak stage.

Both gangue and fracture were products under the influence of material composition and geological structure in the formation process of coal, which reduced the continuity and average degree of mechanical properties of coal. Therefore, both gangue and fracture are called initial damage in this paper. Figure 6 shows the statistical results of peak stress-strain scatter, classified with pink, green, and orange frame lines, which was named as I, II, and III. The three typical failure characteristics of I, II, and III coal cores are shown in Figure 7. According to the results in Figure 7, because of the influence of the initial damage, the strength of the coal had a significant discreteness (5.6~43.6 MPa) and that of some specimens were much higher than the results of the existing study [1] The coal core had lower bearing capacity with a higher degree of initial damage development, but after crushing, the original state of the specimen could still be maintained, and its fragmentation degree was relatively larger, as shown in Figure 7. By contrast, the I coal sample corresponding to the test results in the yellow frame line in Figure 6 with almost no initial damage had a higher strength, and it failed because it could no longer maintain the original state, generally with smaller diameter fragments. The fragment diameter of the medium strength specimen was between that of the high-strength coal sample and the low-strength coal sample. With the test results in the yellow frame line, not only a small diameter fragment but also a large diameter block was included.

To determine the effect of porosity change caused by initial damage on the mechanical properties of coal, the porosity (p) of each coal sample was measured by an experimental method based on equation (1), and the relationship between the strength of the coal and the porosity was obtained:

$$p = \left(1 - \frac{\rho_0}{\rho}\right) \times 100\%, \tag{1}$$

where ρ_0 is the apparent density of coal and ρ is the true density of coal.

In Figure 8, the black scatter is peak stress ($\sigma_{\max}$) of the coal sample and its logarithm of porosity ($\ln p$), and the red line is the linear fitting result of the tow parameters. The results show that there is a linear negative correlation between the strength of the coal and the logarithm of porosity, and this correlation can be expressed as equation (2), indicating that when there are more pores and cracks in the coal, the strength obviously decreases.

$$\sigma_{\max} = a + b \ln p, \tag{2}$$

where a is the maximum strength of the undamaged coal, MPa, and b is the influence coefficient. The former is the characterization of the nature of the coal matrix, and the latter is affected by the orientations of pore fissure development,

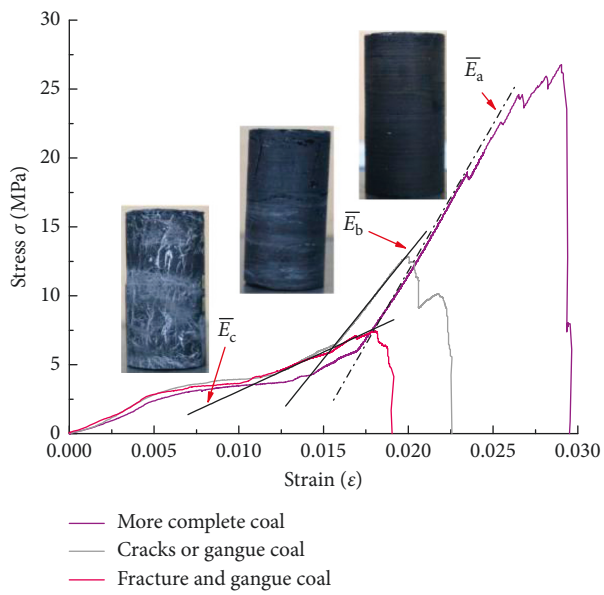

Figure 5: Stress-strain curves of three types of coal affected by gangue and fracture. The result of more complete coal is denoted by the purple curve, cracks, or gangue by the grey curve, and fracture and gangue by the pink curve.

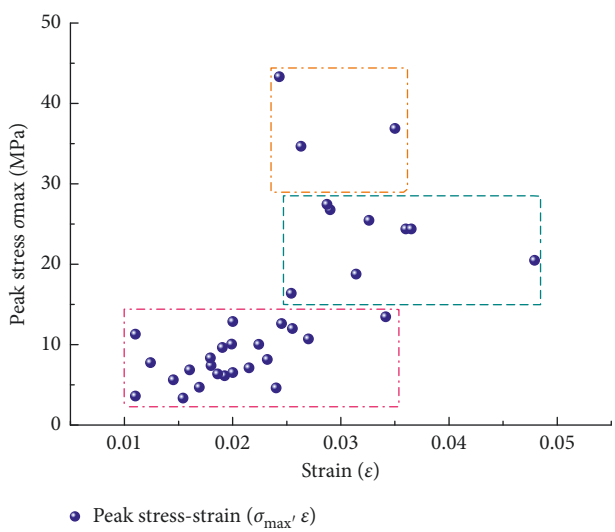

Figure 6: Result of peak stress and strain scatter of coal samples.

principal stress, and the filling material properties of pores-cracks. The more the initial damage of coal sample, the higher the values that are obtained. We thought that the strength prediction was based on equation (2).

For the coal specimen, the interior represents the state of coexistence of the coal matrix particles and pore-crack. The measured results of the computed tomography (CT) scan of coal samples with different porosities are shown in Figure 9, in which the darker areas of the image show the initial damage formed by the pore-crack, where the higher the porosity of the coal, the larger the darker areas, and its characteristics show a rough representation as shown in Figure 10.

In Figure 10, when the coal sample is under uniaxial compression, its total axial load area is S, the actual area under load is S_t, and the area of the nonbearing part of the pore and fracture structure is S_p. Combined with equation (1), the porosity can be further deformed as follows:

$$p = \frac{\rho - \rho_0}{\rho} = \frac{(m/S_t l) - (m/Sl)}{(m/S_t l)} = 1 - \frac{S_t}{S}, \tag{3}$$

where m is the total mass of coal and l is the length of the sample. According to Borberg's definition of the damage variable (D), which is the ratio of effective area ($A(\sim)$) to total area (A),

$$D = \ln\frac{A}{\overline{A}}. \tag{4}$$

Then, according to equation (4), intimal damage variable (D_i) is affected by initial porosity (p_i) and can be expressed as follows:

$$D_i = \ln\left(\frac{1}{1 - p_i}\right). \tag{5}$$

At any time during the loading process, the length of the coal sample is l', and the average radial area is S'. According to the definition of volume strain (ε_v), ε_v can be expressed as follows:

$$\varepsilon_v = \frac{V' - V}{V} = \frac{S'l'}{Sl}. \tag{6}$$

At this moment, the corresponding porosity (p') can be expressed as follows:

$$p' = 1 - \frac{\rho_0}{\rho} = 1 - \frac{\rho_0}{m/(S'l')}. \tag{7}$$

Combining equations (3), (4), (6), and (7), then the damage variable (D) of the coal sample that includes the initial porosity (p_i) and volume strain (ε_v) under uniaxial compression condition can be expressed as follows:

$$D = \ln\left(\frac{1}{(\varepsilon_v + 1)(1 - p_i)}\right). \tag{8}$$

The consequences shown in Figure 11 are the theoretical results of the axial-volumetric strain, stress-strain curve, and damage variables based on the volumetric strain of the coal samples with different initial porosities expressed in the blue lines. The failure of coal is caused mainly by tensile failure under uniaxial conditions, and the opening of cracks will produce lateral expansion in the radial direction. Therefore, evolution of volume is not only elastic expansion of the matrix but also formation and expansion of cracks. According to the characteristics of the volumetric strain with axial strain, the stress-strain curve is divided into 4 stages as follows: In the volume compression phase (~a), volumetric strain is positive and increased slowly due to the microcracks that were perpendicular to the axial direction or a large angle closed by stress and it no longer increases after crack compression. In the volume slow expansion phase (a~b), the sample volume remains in compression, but it decreases slowly with a small

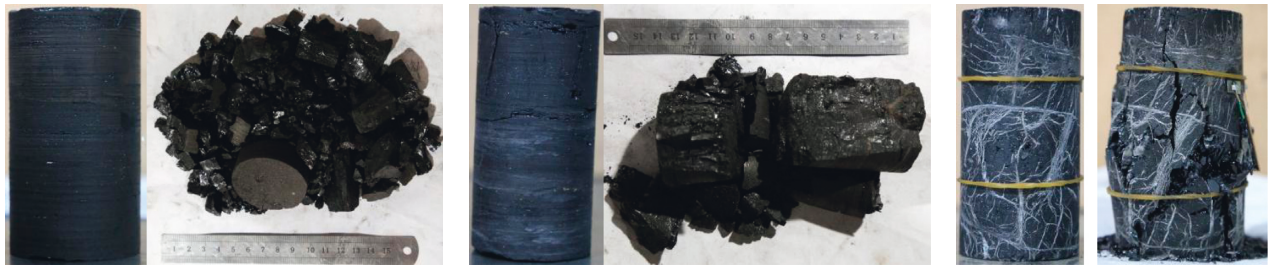

(a) (b) (c)

Figure 7: Failure characteristics of coal with different porosities. (a) Specimen 2# with p = 2.92% in group I. (b) Specimen 9# with p = 4.99% in group II. (c) Specimen 22# with p = 7.88% in group III.

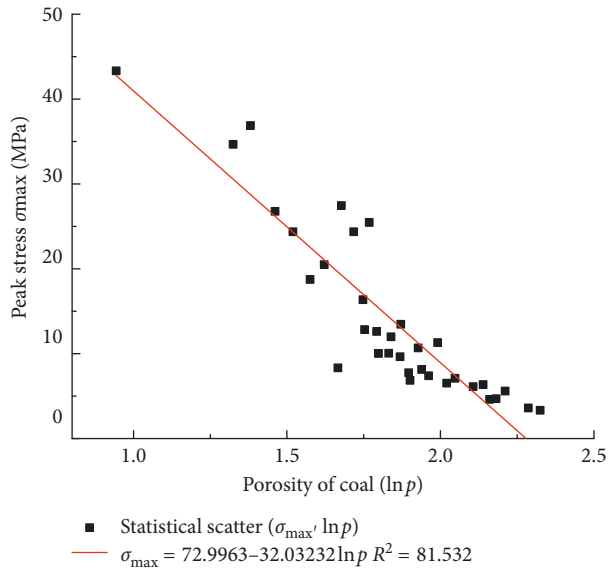

Figure 8: Relationship between peak stress of coal and porosity. The fitting line is denoted by the red line and the measured results by the black scatter.

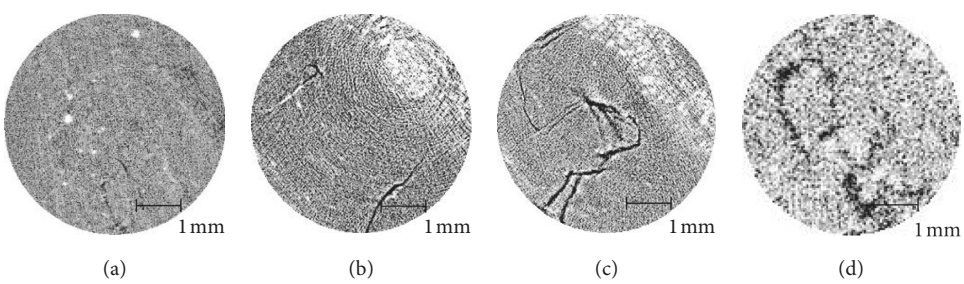

Figure 9: CT scan results of small-size coal samples (Φ5 × 15 mm) with different porosities. (a) p = 3.22%; (b) p = 5.81%; (c) p = 7.54%; (d) p = 8.84%.

variable in the micro-crack-formed expansions, which were parallel to the axial or a small angle and more elastic strain inflation to offset the reduction in the axial strain. In the volume stable expansion phase (b~c), the volumetric strain decreases to negative with a larger fixed value, indicating that the coal sample changed from compressed to expanded. During this process, there were the significant cracks opened that transformed from microscopic to macroscopic and stable elastic deformation of the coal matrix. In the volume rapid expansion phase (c~), when many macroscopic cracks were formed, expansion and destruction occurred under the action of stress. As a result, there was an obviously increased volumetric strain in each stress fluctuation. Additionally, the division of the loading stage based on volumetric strain was basically the same as the stress-strain relationship of compaction (~a), elasticity (a~c), strengthening, and softening (c~). The division of loading stage can also reflect the mechanical evolution inside coal failure, which is verified

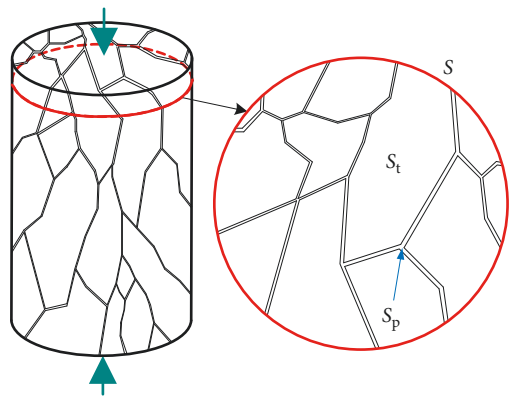

Figure 10: Schematic diagram of internal characteristics of coal block.

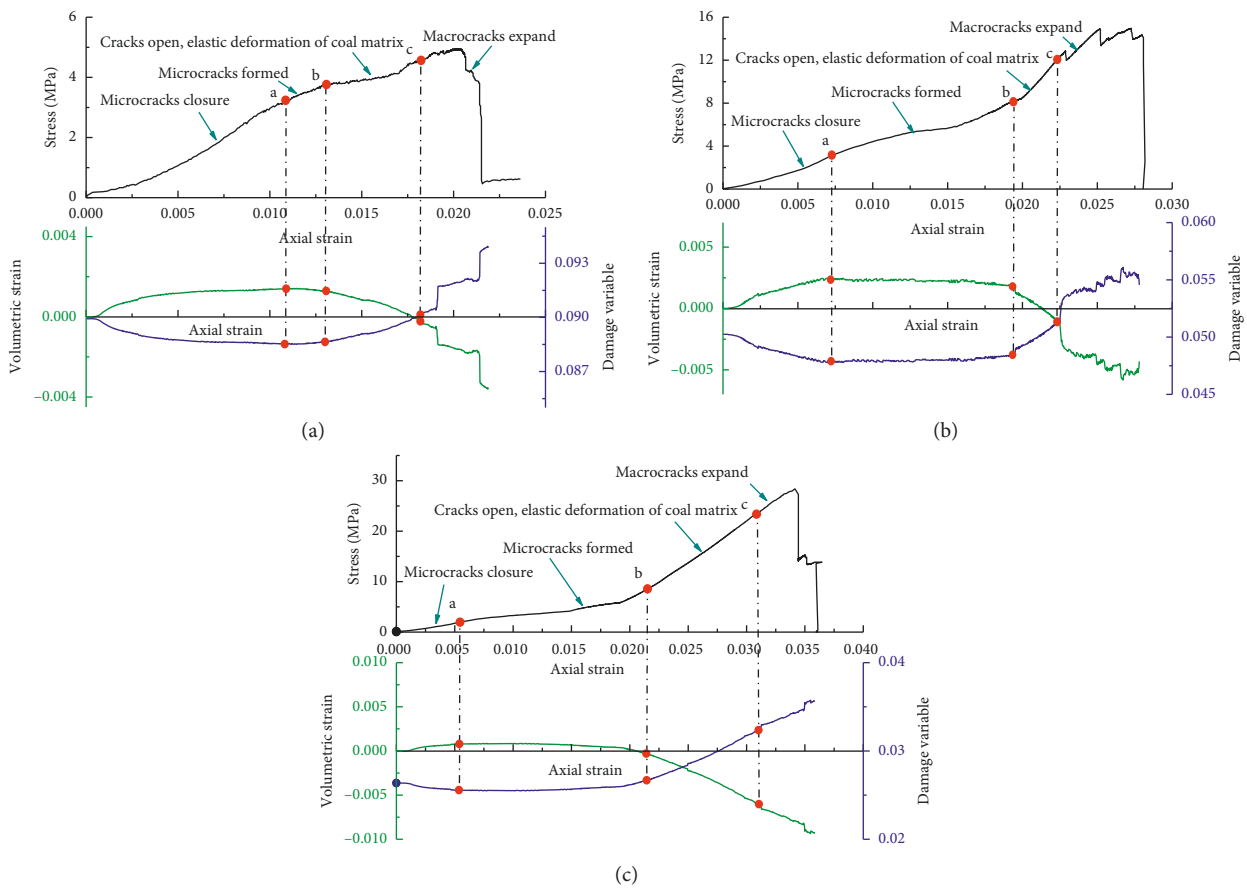

Figure 11: Damage variable evolution with stress and axial and volumetric strain of coal with different initial porosities under uniaxial compression. (a) Specimen 21# with p_i = 8.56% in group III; (b) specimen 9# with p_i = 4.99% in group II; (c) specimen 4# with p_i = 2.59% in group I. In the figures, stress is denoted by the black curve, volumetric strain by the olive curve, and damage variable by the blue curve.

identically by the result [31]. The results illustrated that when the sample has a higher intimal porosity, there are a larger volume compression at point a, a higher increment of slow volume expansion between a and b, a lower stable growth rate of the volumetric strain between b and c, and a smaller final volumetric strain. The stable growth rate of the sample 21# is 0.253, 9# is 0.71, and 4# is 0.786.

The theoretical result of the damage variable demonstrated the variation of decrease (~a), slow increase (a~b), stable rise (b~c), and extreme elevation (c~) at the four stages, similar to the characteristics of volumetric strain in the four stages. The damage variable was directly related to the effective loaded area, which caused cracks to open and extended the stress, which was the key issue for discussion. With cracks, the coal sample more or less had initial damage, and the curve of the damage variable-axial strain had an origin value proportional to porosity. They closed the external loading, and the damage factor decreased, as expected. There was a larger reduction of the damage variable and a longer compact strain with a higher porosity of the coal

sample. After the last process, with a low stress level, where the microcracks formed and extended, the volume of coal no longer decreased and turned from compression to expansion. With the stress improving, cracks were formed along the weak area first and developed into macroscopic main fractures until failure. Then, the damage variable presented as three stages of slow increase, steady growth, and agglomeration. The slope and value were directly affected by the rates and amount of crack development in each stage. When the pores and fracture in coal are developed, there are many more microcrack extensions but a small number of through cracks formed along the direction of the lower fracture toughness, which is most prone to expansion. The growth rate of the damage variable was higher in a~b, but lower in b~c, c~, and smaller total increments of the damage variable. However, coal samples with lower porosity and fewer primary microcrack extensions at the initial loading stage formed many more cracks and perforation until final destruction. As a result, the growth rate of the damage variable was lower in the former but higher in the latter, with a larger total increment of the damage variable. This result also provided a better explanation for the phenomenon mentioned in Figure 7, that the porosity of coal negatively correlated with the destruction level.

The measured result of the damage variable obtained according to equation (8) reflected the evolution of damage caused preferably by crack propagation, but it did not measure up to the ideal value of $D = 1$ as the general theoretical derivation. According to Rabotnov's definition of the damage variable, D [32, 33] is the ratio of the defect area to the nominal, which is expressed by equation (9). In the process of coal failure, any section will not be filled with defects formed by cracks ($0 < A/A < 1$). The conclusion that "when $D < 1$, the damage has already occurred" has been elaborated in the literature [33]. However, this elaboration does not mean that the definition of $D = 1$ at the final destruction of the samples is invalid. The damage factor can be regarded as the ratio of the total defect area formed by the defects in each section projected onto the ideal load-bearing surface, which is perpendicular to the main stress, and the total area, as shown in Figure 12(a) and investigated by You et al. [34] who confirmed that the projection of the final fracture surface perpendicular to the axial direction of the rock sample at least covers its end area. Therefore, the application of theoretical criteria in macroscopic measurement results still needs to be studied further. In this paper, the result of the damage variable was based on the volume strain, which was obtained by the strain gauge of electrical resistance fixed on the surface of samples, as shown in Figure 12(b), that reflected the damage of the corresponding section with a smaller variation according to equation (8). Then, there was a difference from the theory. In general, the calculation in equation (8) of the damage variable, which introduced the volumetric strain and the initial porosity, was a new quantitative description of measured values and damages constructed.

$$D = 1 - \frac{\widetilde{A}}{A}. \tag{9}$$

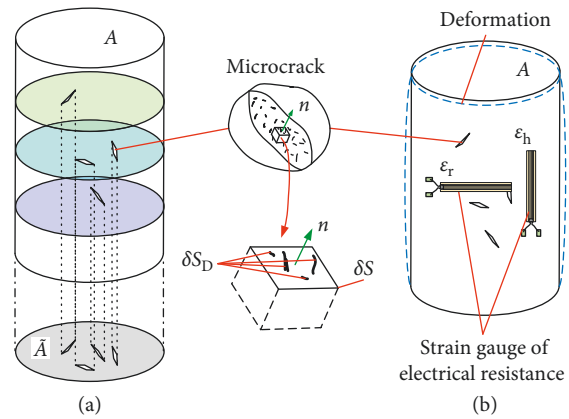

Figure 12: Schematic diagram of damage variable. (a) Theoretical derivation; (b) calculation method in this paper.

The effective stress ($\widetilde{\sigma}$) in coal is expressed as follows:

$$\begin{aligned}\sigma &= \frac{\sigma}{1-D} = \frac{\sigma}{1-\ln\left(1/\left(\left(\varepsilon_v+1\right)\left(1-p_i\right)\right)\right)} \\ &= \frac{\sigma}{1+\ln\left(\left(\varepsilon_v+1\right)\left(1-p_i\right)\right)}.\end{aligned} \tag{10}$$

The tensile failure of coal under uniaxial conditions is due to the shear slip of the coal matrix. Then, the Mohr–Coulomb criterion is introduced and is expressed by effective stress as follows:

$$\tau = c + \frac{\sigma \tan \varphi}{1+\ln\left(\left(\varepsilon_v+1\right)\left(1-p_i\right)\right)}, \tag{11}$$

where τ is shear stress, c is cohesive force, and φ is the internal friction angle. According to the result of the expression in equation (11), the larger the porosity and volume strain of coal rock, the greater the shear stress inside.

Let us evaluate the stress state of a representative elementary volume of a coal sample through its Mohr circle. Figure 13 shows a series of Mohr's stress circles and the failure envelope that illustrates the proposed failure mechanism. The explanation is summarized as follows: under normal conditions, the Mohr circle and its failure envelope are expressed by the blue line. Due to the existence of weak gangue, the continuity of the coal matrix decreased, which makes it have a smaller cohesive force (c') and internal friction angle (φ'). The Mohr circle and its failure envelope are expressed by the green line. However, the actual shear stress growth induced by the initial damage is increased, and there is volume expansion until a situation in which shear failure may occur. The Mohr circle of the coal sample is expressed in the red line, its radius by equation (11). The higher the porosity of the coal, the larger the radius of the Mohr circle. The Mohr circle is more likely to be destroyed, which highlights the fact that more pores and fractures in coal can accelerate the failure, as shown in Figure 8.

$$R = \sqrt{\frac{\sigma^2}{4}+\tau^2} = \sqrt{\frac{\sigma^2}{4}+\left(c' + \frac{\sigma \tan \phi'}{1+\ln\left(\left(\varepsilon_v+1\right)\left(1+p_i\right)\right)}\right)}. \tag{12}$$

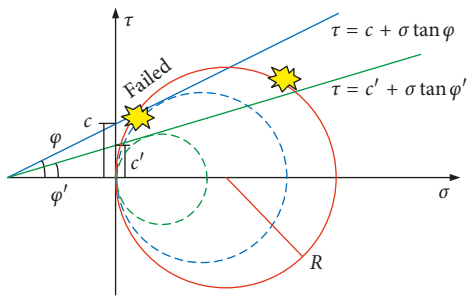

Figure 13: Mechanism for failure of coal samples in terms of porosity and its effects on the internal friction angle, cohesion: 2D Mohr circle.

3.2. Characteristics of Acoustic Emission-Charge Induction of Bump-Prone Coal with Different Porosities. In Figures 14 and 15, the variations of acoustic emission (AE) energy, charge induction pulse, and their accumulation are presented, which was the result from a coal sample with low, moderate, and high strength selected from the strength series.

A notable law of AE and charge signal existed, even though the strengths of the coal samples were different. We divided the stress curve into three stages of stable loaded, microcrack forming-extending, and macrocrack extending, based on the distribution of the signal:

(1) Stable loaded stage: the stress shows a gradual decline caused by the original fracture gradually closing with the increase in loading. During this process, there was some weak acoustic emission signal and no charge pulse appearance, for the accumulation curves were rendered as two nearly horizontal lines. This phenomenon indicated that the original fracture closed without energy release, and no frictional slip occurred between the two faces of the crack.

(2) Microcracks forming-extending stage: the amplitude of AE is generally in a lower range of 1.0×10^4 mV/μs, indicating that the microcracks have been gradually sprouting and slowly expanding, while the charge signal is expressed as a small amplitude and sporadic pulse, and the accumulation curves of two signals grow slowly with a smaller slope.

(3) Macrocrack extended stage: the high-amplitude signal of AE density appeared continuously, and its average value was generally greater than 1.0×10^4 mV/μs. Until the loading reached the first peak stress, the high-amplitude charge signal appeared continuously, and then for both the acoustic emission and charge signal, there was a high-amplitude pulse at each stress drop.

There was a surge point where both signals had significantly large-amplitude signals and accumulations of them. After this feature point, the distribution characteristics of AE energy and charge accumulation were very similar for the results listed as before. At the peak point, both the acoustic emission and the charge signal appear as the highest value of the entire loading process. The cumulative curve also had a significant growth step at the same time. The continuous high-value signal began to emerge gradually. For both AE energy and charge pulse, the accumulation of AE energy for 3%–8.22% of the total and for the charge was less than 1%, from the stable loaded stage to microcrack forming-extending. The main part of the AE and charge is generated during the macrocrack extending stage, where the curves of accumulation manifest growth, according to the research [12, 13] that acoustic emission reflects the stress wave of crack propagation. The self-potential anomalies in the loading and destruction processes of coal are observed caused by free charges generated, which is the comprehensive result of the piezoelectric effect, the microcrack interface barrier dislocation, and the sliding frictional electricity generation effect between the fracture surfaces, within existing knowledge [23, 35, 36]. To date, however, the primary and secondary nature of several bioelectricity mechanisms remains a key scientific issue that requires a deep research, and our academic view is updated to the sliding friction which is the main electricity generation mechanism; thus, the following discussion suggests that the charge pulse is the free charge of crack friction. Both of the signals are directly related to cracks. Therefore, the greater the physical signal generated in this process, the more cracks were formed and friction inside the coal, also verifying the rationality of the analysis in the previous section. For the surge point of both signals, which is the transition point of signals from small-value fluctuations to high-amplitude oscillation, it means that the size of cracks transformed from microto macro, so it can be regarded as the initial point of new macro damage generated in the coal sample, and this feature point of samples is all in the elastic phase of the stress-strain relationship.

Comparing the results of the three samples, as the strength increased, the amplitude and continuity of acoustic emission and charge induction was improved, with more total accumulation of the acoustic emission and charge induction. Therefore, more information was collected, more cracks were generated in the coal, and the frictional slip became intense, associated with the result in Figure 8 that the higher the strength, the more the cracks formed after the damage and the greater the degree of breakage.

3.3. Results of Acoustic Emission-Charge Signal in the Time-Frequency Domain at the Feature Points of Stress. As AE and charge signals recorded by transducers are the typical nonstationary time domain signals, which are often composed of more than two frequency components, the distribution and amplitude of the uncertainty waveforms in the time domain and the main frequency components correspond to different AE and charge information. Then, the representative results of the typical time domain waveforms and their frequencies obtained by fast Fourier transformation (FFT) to the AE and charge induction for samples $5^{\#}$, $10^{\#}$, and $18^{\#}$ recorded in tests are presented in Figures 16–19, which were at surge and peak point with different stresses affected by initial damage, and their characteristics are simply investigated. In this part, we selected the wavelength of AE as 1 ms, and the charge was 1 s at

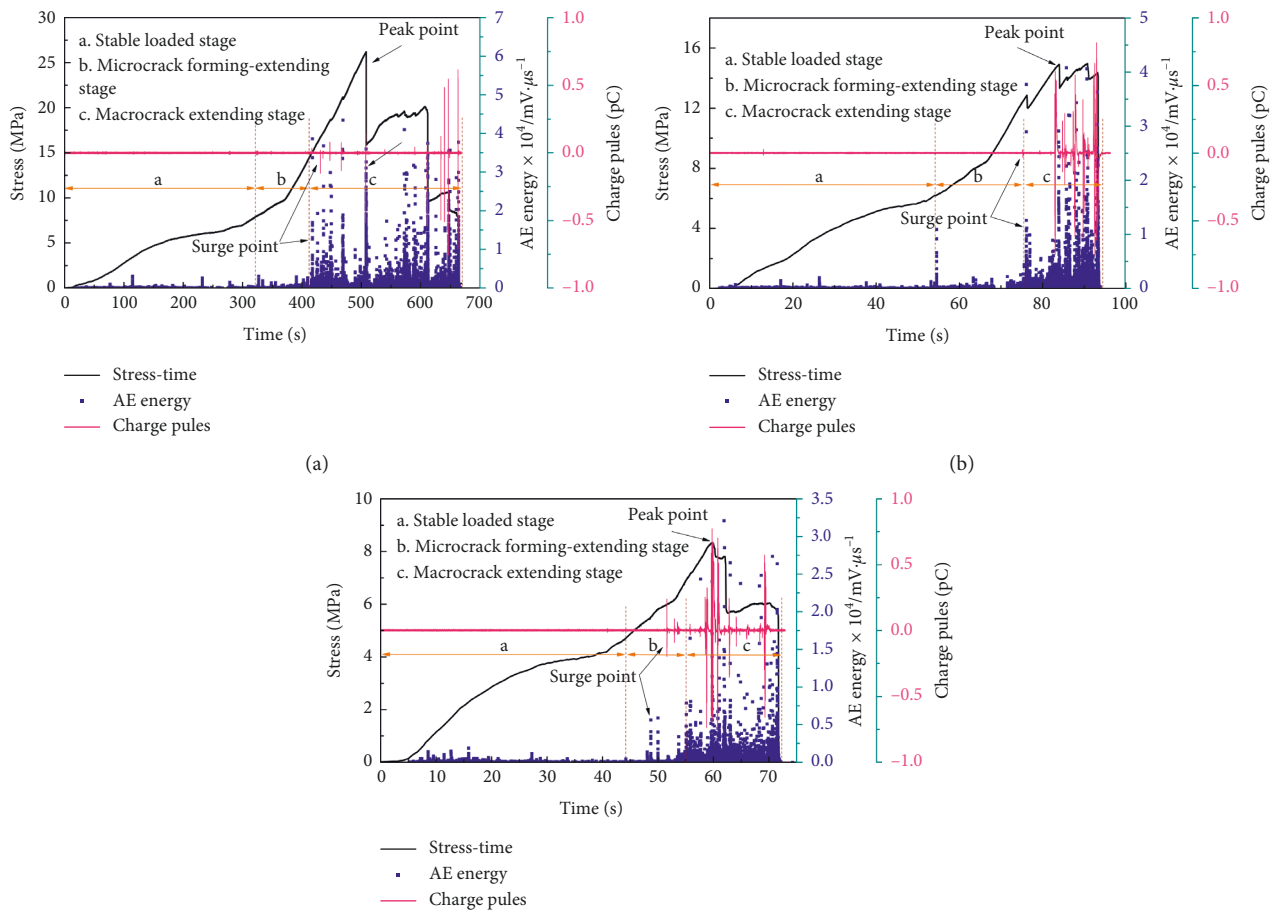

Figure 14: Variation of stress, acoustic emission energy, and charge pulse with time. (a) Specimen 25# with high strength; (b) specimen 9# with moderate strength; (c) specimen 3 # with low strength. Stress is denoted by the black curve, the charge pulse by the pink line, and the AE energy by the blue scatter.

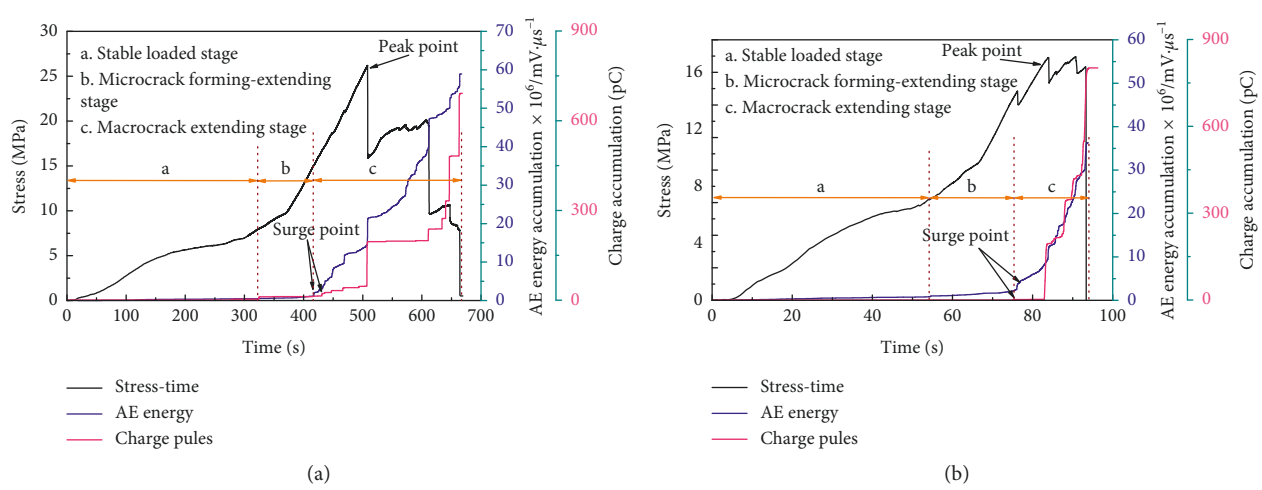

Figure 15: Continued.

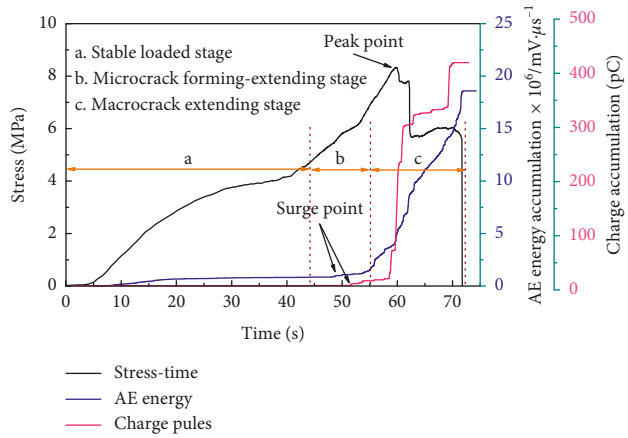

(c)

Figure 15: Variation of stress, accumulation of acoustic emission energy, and charge with time. (a) Specimen 25# with high strength; (b) specimen 9# with moderate strength; (c) specimen 3# with low strength. Stress is denoted by the black curve, the charge accumulation by the pink curve, and the AE energy accumulation by the blue curve.

two feature points. At the signal surge point, the stress of sample 5# is 5.12 MPa, 10# is 9.75 MPa, and 18# is 15.6 MPa. At peak point, the strength of sample 5# is 8.23 MPa, 10# is 16.11 MPa, and 18# is 26.78 MPa.

In general, as the result illustrated in Figures 16(a) and 17(a) shows, the expressions of the time domain waveforms of AE and charge induction are basically similar. Both of them are given priority with small-amplitude fluctuations at the surge point. With stress improved, the small fluctuations in the waveform gradually decrease and turn into high amplitude. Compare the three results for a, b, and c in the figures. For the consequence demonstrated in Figure 16(b) by the frequency spectral analysis of AE that three frequency band components constituted the waveforms, in which the range of the main frequency is 1~50 kHz, subfrequency is 100~150 kHz, and the third frequency is 175~200 kHz, and the amplitude of the frequency components in each band is sequentially decreased correspondingly in turn. As the stress of the surge point increases, the amplitude of the main frequency band improved unexpectedly, the amplitude of the sub and third decreased. For the result presented in Figure 17(b), the waveforms of charge induction monitored shown a low-frequency band of 1~100 Hz and white noise with a certain amplitude and frequency of 150 Hz, 350 Hz (reported in test by [37]). Similarly, the amplitude of the main frequency band is improved with the stress of the surge point increased.

The results of AE and charge induction recorded by transducers are shown in Figures 18(a) and 19(a). The expressions of time domain waveforms of AE and charge induction are presented with high-amplitude fluctuation at the peak point. Furthermore, the large-amplitude waves of the two signals increased significantly and the small-amplitude oscillations that mixed in high-amplitude waveforms significantly decreased with the strength of coal improved. The same situation was demonstrated in Figure 18(b), with a higher stress of the coal. The amplitude of the main frequency obviously improved, and the frequency of the sub and third decreased further. This change was most evident in the spectrum of sample 5#, and the same charge induction, shown in Figure 19(b), which had a distinct growth to the amplitude of the main frequency band, and the frequency of the largest amplitude, was constantly moving forward.

According to the widely recognized fundamental principles of fracture mechanics that cracks in the material are generated and developed along the lowest fracture factor, there were many more weak interlayers and microcracks with a lower fracture factor when the coal sample had more initial damage. Then, cracks emerged with expansion at lower stress, and the stress waves were released by the crack propagation with a high continuity but weakly. As a result, the small-amplitude fluctuations monitored by transducers dominated in three frequency bands of 1~50 kHz, 100~150 kHz, and 175~200 kHz with low amplitude. However, for the coal samples with less initial damage, the propagation concentrated on a small number of cracks, and critical stress improved. Then, the stress wave showed a continuity that was low but powerful. The AE signal dominated in the main frequency band with large amplitude. It is not difficult to find that the phenomenon is more pronounced at the peak point, where the amplitudes and frequencies of AE waveforms indeed vary with the different stresses at the final stage. At the peak point, there were much larger macroscopic cracks formed and extended with a higher stress. Then, more strain energy was released outward and formed into the stress wave with a low-frequency and a high amplitude, and this characteristic is reflected in the same form by the AE waveforms. The test reflected the same results as the previous studies that the amplitudes of the AE waveforms increased as the stress improved. A large-amplitude signal is presented at the final stage, and the frequency distribution is concentrated on low frequency. The same certain differences also existed; that is, the frequency of the waveform recorded in the coal failure (1~50 kHz) is lower than the frequency of the rock samples according to the tests by He et al. [19], Wang et al. [38], and Su et al. [39].

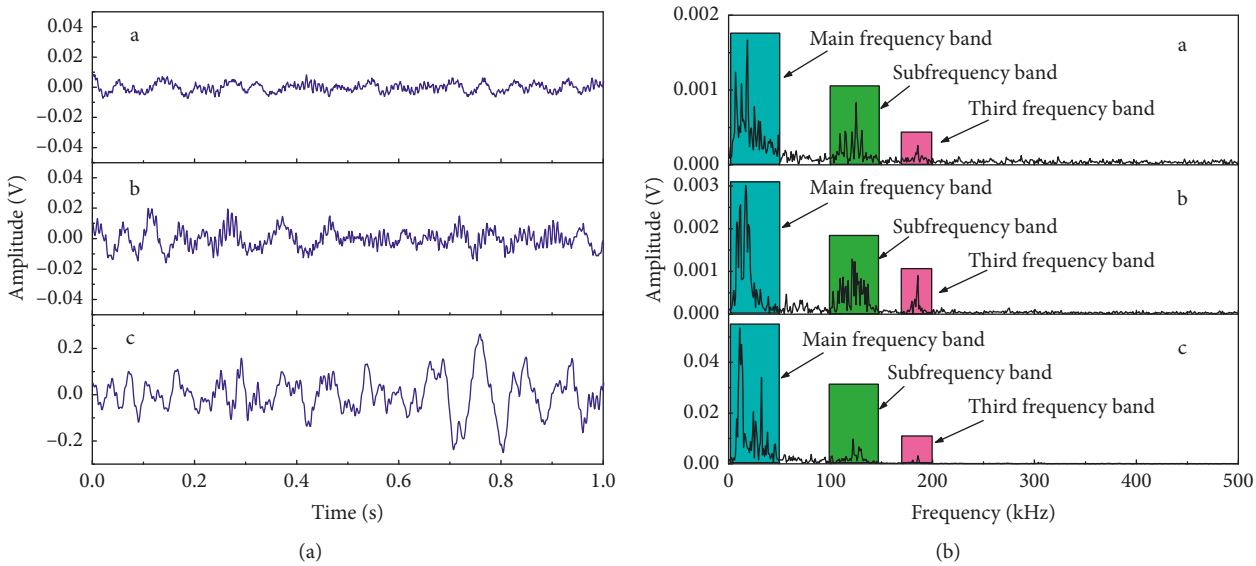

Figure 16: AE waveforms in the time domain and the frequency distribution recorded for the tests at the signal surge point of coal: (a) time domain and (b) frequency. a is specimen #18, b is specimen #10, and c is specimen #5.

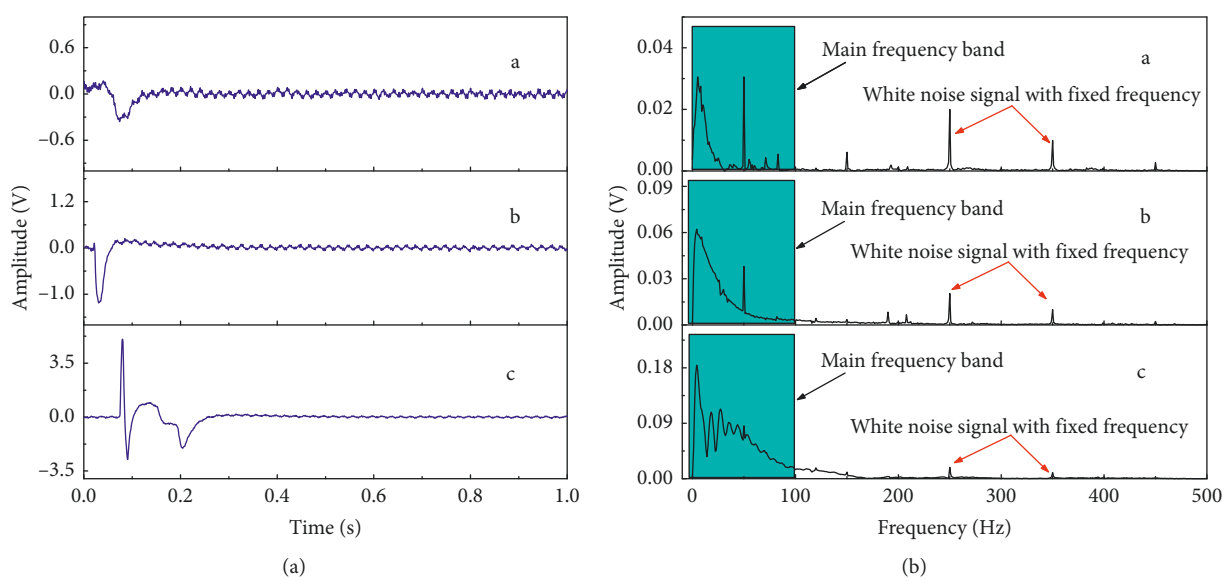

Figure 17: Charge induction waveforms in the time domain and the frequency distribution recorded for the tests at the signal surge point of coal: (a) time domain and (b) frequency. a is specimen 18#, b is specimen 10#, and c is specimen 5#.

The charge induction is the signal monitored for charge anomaly during the failure process of coal. The existence time and amount of charge directly affects the amplitude and frequency of the signal over the range of frequencies that can be monitored. The amount of charge generated by frictional slip between cracks corresponds to the stress according to the tests by Budakian and Putterman [35]. The higher the stress level at the frictional slip occurs, the more the charge is generated. The better the continuity of the charge generated, the longer the duration of the self-potential abnormality of the coal surface and the higher the low-frequency component in the signal, according to the digital sampling theorem. As a result, small-amplitude oscillations occur with lower stress, and the large-amplitude waveforms are presented at the peak point and final stage. The charge induction is a kind of very-low-frequency signal (1~100 kHz), which is the major feature difference from the electromagnetic radiation (EMR) reported by Yamada et al. [24], Rabinovitch et al. [25], and Freund et al. [22].

4. Discussion of the Similarities and Differences between AE and Charge Induction Signals

Many experiments on AE or the charge signal characteristic of coal materials under various conditions have been carried out, most of them concentrated mainly on the

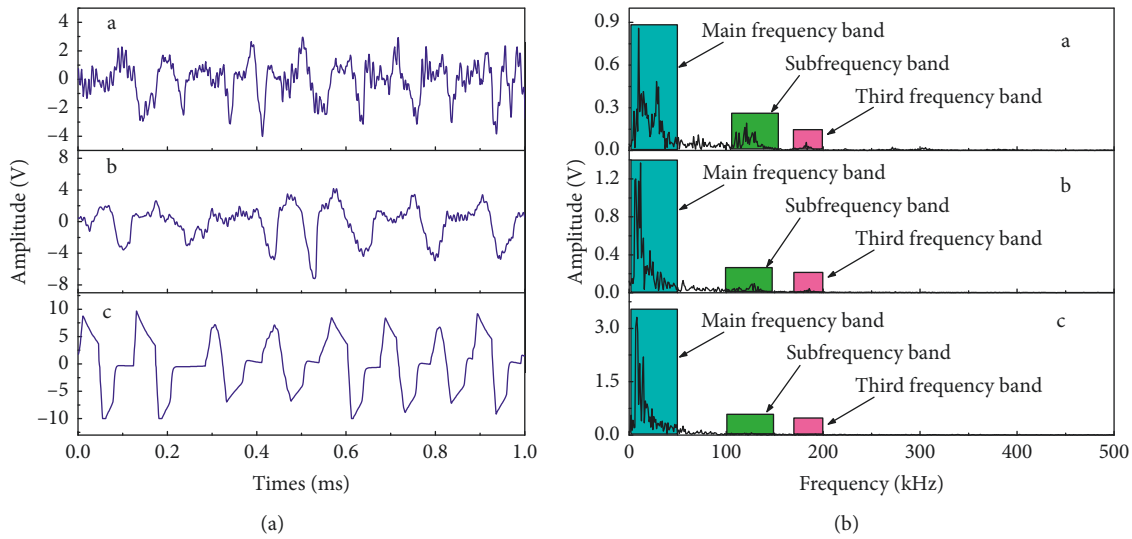

Figure 18: AE waveforms in the time domain and the frequency distribution recorded for the tests at the peak point of coal. (a) Time domain; (b) frequency. a is specimen 18#, b is specimen 10#, and a is specimen 5#.

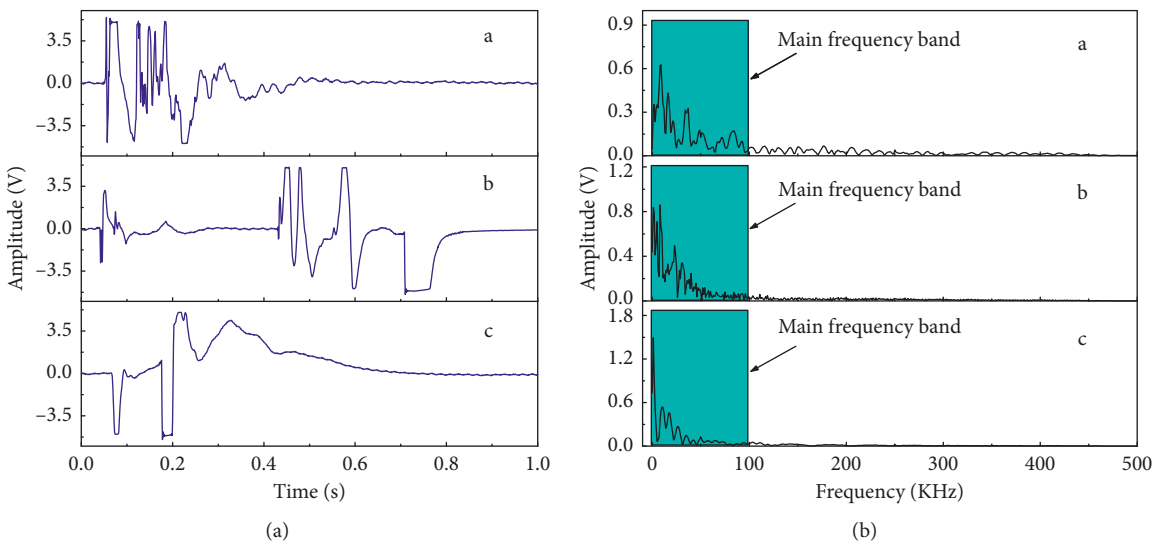

Figure 19: Charge induction waveforms in the time domain and its frequency distribution are recorded for the tests at the peak point of coal. (a) Time domain; (b) frequency. a is specimen 18#, b is specimen 10#, and a is specimen 5#.

evolution of each signal with stress variation, but rarely about the similarities and differences between them in the time and frequency domain of the coal specimens with different porosities before and after the peak. From this study, the internal damage evolution caused by the porosity of the specimens has an important influence on the AE-charge distribution in time and spectrum and is obviously asynchronous in the coal failure process. Fundamentally, the stress wave is generated by crack propagation, and free charge mainly emerges by dislocation between two surfaces of the crack. Meanwhile, the damage and failure of coal is the result of crack evolution from microto macro, including crack initiation, expansion, convergence, and cut-though in coal. Therefore, the clarified same and different characterization of AE or charge induction at an identical loading stage is the key to identifying the crack size and activity, inverse damage variation, and prediction of the instability of coal based on the compound signal of the two methods.

The curves of stress, AE energy, AE energy accumulation, charge pulse, and charge accumulation with time before and after the peak and stress drop at the peak are shown in Figures 20 and 21, which were the enlarged view of the typical result for coal loaded, no matter whatever the porosity of the specimen is. Before the peak phase, the stress stable increased, and the AE signal was produced at the beginning of a small stress fluctuation, but the charge pulses were generated randomly when the first stress fluctuation appeared, as described above. At the post stage, the AE signal emerged at the beginning of the stress drop, while the charge pulse was produced with the stress drop. For accumulations of the two signals, the AE was assumed to be an inclined line

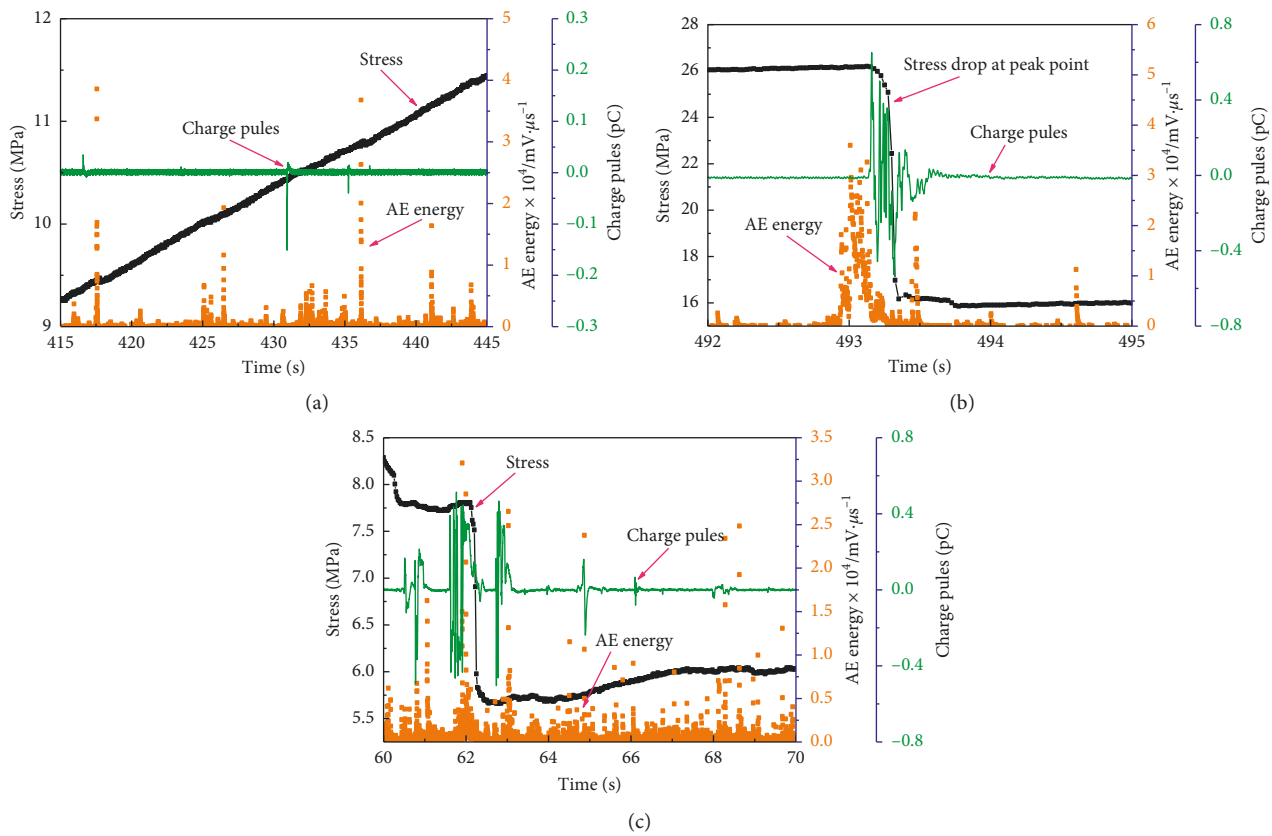

Figure 20: Test result of AE and charge induction signal for coal specimen under uniaxial compression at a different stages. (a) Before peak; (b) peak point; (c) after peak. Stress is denoted by the black curve, AE energy by the orange scatter, and charge pulse by the thin green line.

with a certain slope when the charge is stepped up, both before and postpeak. It is worth to note that, with the stress drop at peak, the signal reached the highest value of hole loading process, the accumulations of them were assumed to be an obviously stepped up, and AE appears before charge pulse also. As a result, there is a significant asynchrony between the AE signal and the charge pulses during the coal failure process.

The asynchronous phenomenon between the two signals indicates that both originated from cracks in coal, and they belong to homologous signals, but there are different manifestations for crack evolution, due mainly to the different production mechanisms. When crack propagation occurs in coal, there will be elastic energy release and transformation into a stress wave monitored in the form of an AE signal. The larger the scale and the more active the crack expansion, the higher the amplitude and the more signal is recorded. When the friction between the two faces of the crack is weak, and there is no or little charge generated, as a result, the monitoring signal shown has no or a low-amplitude pulse. In contrast, it is a violent interaction on the faces of the crack, and there is much more free charge produced. The pulse with the large amplitude and long wavelength is recorded, which is most obvious at the stress drop in the postpeak stage, as shown in Figure 20(b), which is also confirmed in the studies [40, 41]. We conclude that crack development is bound to be accompanied by a stress wavelet, not necessarily free charge. Meanwhile, charge pulses being emerging means there must be crack interaction. Both of them are directly related to cracks, but the acoustic emission signals are generated prior to charge induction.

Therefore, we can determine the damage development of coal preliminarily based on the distribution characteristics of acoustic emission and charge induction. The amplitude and continuity of AE is used to judge the crack activity, and the amplitude and continuity of charge induction determines the loading stage. In addition, the main frequency bands of the two signals are used to consider whether the message source is cracks or power frequency interference. In addition, the accumulation of the signals is also an important parameter. In particular, the slope increases, and the faster the cumulative amount of signal grows in the same time, the more active the number of the cracks in coal for both the AE and charge induction. In general, the diversity of AE and the charge precursor is the external illustration of crack propagation and is beneficial information for the coal mass instability forecast. Furthermore, in addition to the parameters mentioned in this paper, others also need to be investigated in depth, especially the charge induction as a new monitoring method. The beneficial signal extraction methods and monitoring equipment must be further improved. How to

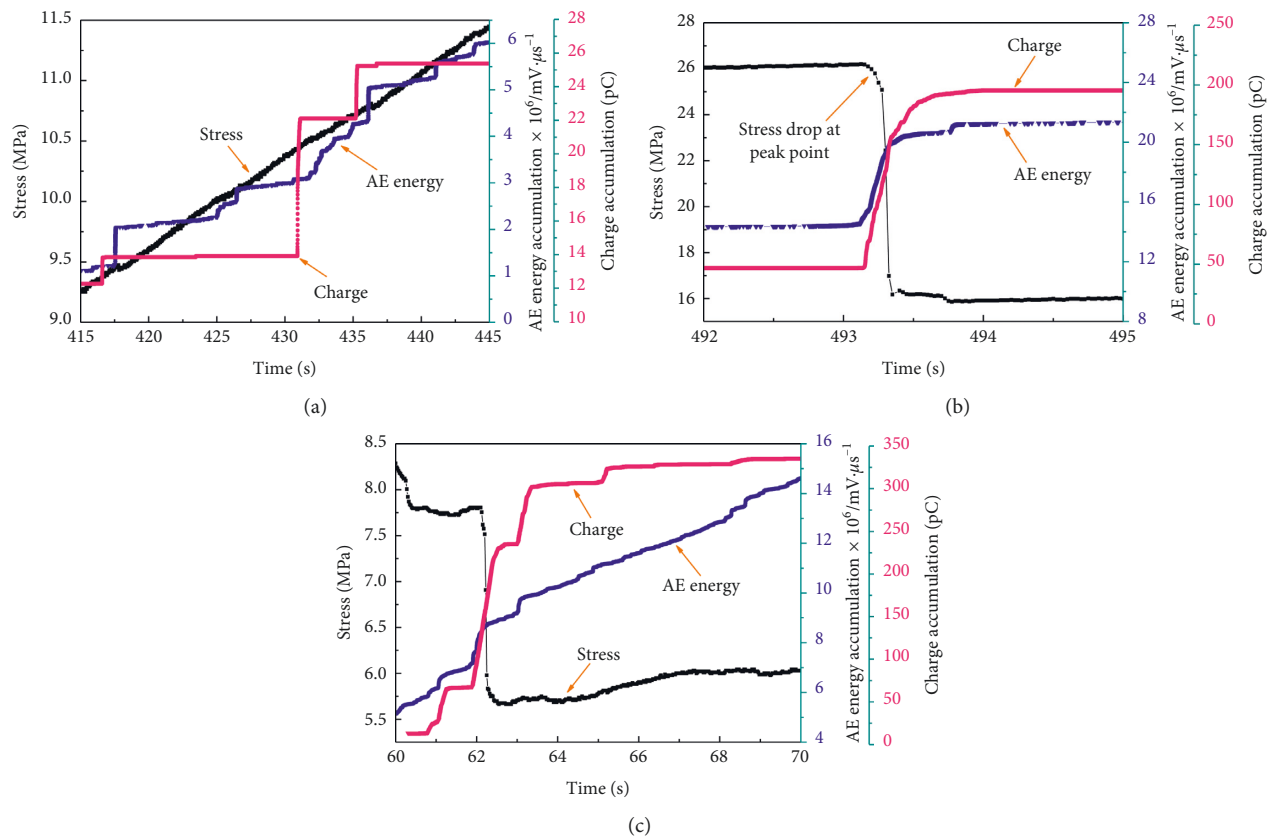

Figure 21: Test result of AE energy and charge accumulations for coal specimen under uniaxial compression in different stages. (a) Strengthening stage before peak; (b) peak point; (c) after peak. Stress is denoted by the black curve, AE energy accumulation by the blue curve, and charge accumulation by the thin pink line.

make a better use of the diverse responses of different signals to cracks and loading stage for coal is the key to the compound signal monitoring method, which should be considered for future study.

5. Conclusions

In this paper, a uniaxial compression experiment was carried out to investigate the mechanical properties of coal samples with different porosities and their characteristic AE events and charge induction pulse during the failure process, together with some auxiliary systems such as CT and FFT analysis. Based on the results and discussion, the following conclusions can be established.

Initial damage caused by gangue and fracture in coal is presented by CT, which emerged affected with various degrees of material composition and geological structure that reduce the continuity and homogeneity of specimens. As a result, there is a linear negative correlation between the strength of the coal and the logarithm of porosity, and the elastic modules decrease with the initial damage increasing. With the introduction of the theory of damage mechanics, a new quantitative description of the damage variable based on volumetric strain and initial porosity was established by theoretical derivation, reflecting the evolution of damage caused by crack propagation during the entire loading process and explaining the failure characteristics of the coal samples preferably affected by porosity. According to the principle of Mohr–Coulomb, the higher the porosity of the coal sample, the greater the initial damage, and the effective stress is more likely to reach the shear strength and destruction. Thus, the porosity structure characteristics of coal are an important consideration not only in discussing gas migration but also in analysing the discreteness of mechanical properties for coal mass underground bump-prone judgement.

The amplitudes and accumulation of AE energy and charge pulse indeed vary with the stress loading stages. The signal begins to appear in the stage of elasticity or strength and is concentrated in the failure stage after the peak. As the strength of the coal sample increases, the amplitude and continuity of AE and charge signals improve, with more total accumulation. The frequency of the AE waveform dominates in three bands (1~50 kHz, 100~150 kHz, and 175~200 kHz), and charge induction had one frequency band at 1~100 Hz. The amplitudes of the main frequency components improved with increased stress. Both originated from cracks and belong to homologous signals. Crack development is bound to be accompanied by a stress wavelet, not necessarily free charge. Meanwhile, charge pulses emerging means there must be crack interaction. The acoustic emission signals are generated prior to charge induction. Insight into the characteristics of AE and charge induction of coal failure is basic for the establishment of an AE-charge compound

signal monitoring system for the assessment of coal bump in deep underground energy source exploration.

Nomenclature

ρ_0 (g/cm^3): Apparent density of coal
ρ (g/cm^3): True density of coal
p: Porosity
σ_{max} (MPa): Peak stress of coal sample
a (MPa): Maximum strength of undamaged coal
b: Influence coefficient
S (cm^2): Total axial load area
S_t (cm^2): Actual load area
m (g): Total mass of coal
l (cm): Original length of sample
D: Damage variable
$A(\sim)$ (cm^2): Effective load area
A (cm^2): Total area
D_i: Intimal damage variable
p_i: Initial porosity
l' (cm): Length of sample during loading
S' (cm^2): Average radial area
ε_v: Volume strain
p': Porosity of coal during loading
$\tilde{\sigma}$ (MPa): Effective stress
τ (MPa): Hear stress
c (MPa): Cohesive force
φ (°): Internal frication angle.

Data Availability

The figures data used to support the findings of this study are included within the article.

Conflicts of Interest

The authors declare no conflicts of interest.

Acknowledgments

This work was supported by the National Key Research and Development Program of China (no. 2017YFC0804208), the National Natural Science Foundation of China (nos. 51774164, 51774048, and 51504122), and the Scientific Research Foundation of State Key Lab. of Coal Mine Disaster Dynamics and Control (2011DA105287-FW201605).

References

[1] M.-T. Zhang, Y.-S. Pan, B. Liang, and L.-G. Wang, *Coal and Rock Fluid Mechanics*, China Science Publishing & Media Ltd, Beijing, China, 1995, in Chinese.

[2] C. Ö. Karacan and E. Okandan, "Fracture/cleat analysis of coals from Zonguldak basin (northwestern Turkey) relative to the potential of coalbed methane production," *International Journal of Coal Geology*, vol. 44, no. 2, pp. 109–125, 2000.

[3] Y.-S. Pan, Z.-H. Li, and M.-T. Zhang, "Distribution, type, mechanism and prevention of rockbrust in China," *Chinese Journal of Rock Mechanics and Engineering*, vol. 22, no. 11, pp. 1844–1851, 2003, Chinese in English Abstract.

[4] D. W. van Krevelen, *Coal: Typology-Physics-Chemistry-Constitution*, Elsevier, Amsterdam, Netherlands, 3rd edition, 1993.

[5] C. I. Pattinson, C. R. Fielding, R. H. McWatters, and L. H. Hamilton, "Nature and origin of fractures in Permian coals from the Bowen basin, Queensland, Australia," in *Coalbed Methane and Coal Geology*, Gaye, Ed., vol. 109, pp. 133–150, The Geological Society, Special Publication, London, UK, 1996.

[6] T. Zhao, Z. Zhang, Y. Tan, C. Shi, P. Wei, and Q. Li, "An innovative approach to thin coal seam mining of complex geological conditions by pressure regulation," *International Journal of Rock Mechanics and Mining Sciences*, vol. 71, pp. 249–257, 2014.

[7] A. K. Ray, G. S. P. Singh, and G. Banerjee, "Influence of petrographic constituents on the softening characteristics of coal measures rocks," *International Journal of Rock Mechanics and Mining Sciences*, vol. 43, no. 3, pp. 494–502, 2006.

[8] P. Konecny and A. Kozusnikova, "Influence of stress on the permeability of coal and sedimentary rocks of the upper Silesian basin," *International Journal of Rock Mechanics and Mining Sciences*, vol. 48, no. 2, pp. 347–352, 2011.

[9] L. Mao, P. Shi, H. Tu, L. An, Y. Ju, and N. Hao, "Porosity analysis based on CT images of coal under uniaxial loading," *Advances in Computed Tomography*, vol. 1, no. 2, pp. 5–10, 2012.

[10] Y. Cai, D. Liu, J. P. Mathews et al., "Permeability evolution in fractured coal—combining triaxial confinement with X-ray computed tomography, acoustic emission and ultrasonic techniques," *International Journal of Coal Geology*, vol. 122, pp. 91–104, 2014.

[11] M. Klawitter, J. Esterle, and S. Collins, "A study of hardness and fracture propagation in coal," *International Journal of Rock Mechanics and Mining Sciences*, vol. 76, pp. 237–242, 2015.

[12] Y. Niwa, S. Kobayashi, and M. Ohtsu, "Source mechanisms and wave motions of acoustic emission in rock-like materials," in *Proceedings of the Third Conference on Acoustic Emission/Microseismic Activity in Geologic Structures and Materials*, pp. 101–115, Trans Tech Publications, University Park, PA, USA, October 1981.

[13] C. H. Sondergeld, L. A. Granryd, and L. H. Estey, "Acoustic emissions during compression testing of rock," in *Proceedings of the Third Conference on Acoustic Emission/Microseismic Activity in Geologic Structures and Materials*, pp. 131–145, Trans Tech Publications, University Park, PA, USA, October 1981.

[14] Y. Enomoto and H. Hashimoto, "Emission of charged particles from indentation fracture of rocks," *Nature*, vol. 346, no. 6285, pp. 641–643, 1990.

[15] V. Rudajev, J. Vilhelm, and T. Lokajíček, "Laboratory studies of acoustic emission prior to uniaxial compressive rock failure," *International Journal of Rock Mechanics and Mining Sciences*, vol. 37, no. 4, pp. 699–704, 2000.

[16] V. L. Shkuratnik, Y. L. Filimonov, and S. V. Kuchurin, "Experimental investigations into acoustic emission in coal samples under uniaxial loading," *Journal of Mining Science*, vol. 40, no. 5, pp. 458–464, 2004.

[17] A. V. Lavrov and V. L. Shkuratnik, "Deformation-and fracture-induced acoustic emission in rocks," *Acoustical Physics*, vol. 51, no. S1, pp. S2–S11, 2005.

[18] F.-Q. Su, K.-I. Itakura, G. Deguchi, and K. Ohga, "Monitoring of coal fracturing in underground coal gasification by acoustic emission techniques," *Applied Energy*, vol. 189, pp. 142–156, 2017.

[19] M. C. He, J. L. Miao, and J. L. Feng, "Rock burst process of limestone and its acoustic emission characteristics under true-triaxial unloading conditions," *International Journal of Rock Mechanics and Mining Sciences*, vol. 47, no. 2, pp. 286–298, 2010.

[20] H. Yang, G. Wen, Q. Hu, Y. Li, and L. Dai, "Experimental investigation on influence factors of acoustic emission activity in coal failure process," *Energies*, vol. 11, no. 6, p. 1414, 2018.

[21] V. S. Kuksenko, K. F. Makhmudov, and A. V. Ponomarev, "Relaxation of electric fields induced by mechanical loading in natural dielectrics," *Physics of the Solid State*, vol. 39, no. 7, pp. 1065-1066, 1997.

[22] F. T. Freund, A. Takeuchi, and B. W. S. Lau, "Electric currents streaming out of stressed igneous rocks—a step towards understanding pre-earthquake low frequency EM emissions," *Physics and Chemistry of the Earth*, vol. 31, no. 4–9, pp. 389–396, 2016.

[23] X. Lv, Y. Pan, X. Xiao, and A. Wang, "Barrier formation of micro-crack interface and piezoelectric effect in coal and rock masses," *International Journal of Rock Mechanics and Mining Sciences*, vol. 64, pp. 1–5, 2013.

[24] I. Yamada, K. Masuda, and H. Mizutani, "Electromagnetic and acoustic emission associated with rock fracture," *Physics of the Earth and Planetary Interiors*, vol. 57, no. 1-2, pp. 157–168, 1989.

[25] A. Rabinovitch, D. Bahat, and V. Frid, "Comparison of electromagnetic radiation and acoustic emission in granite fracturing," *International Journal of Fracture*, vol. 71, no. 2, pp. R33–R41, 1995.

[26] D. Eccles, P. R. Sammonds, and O. C. Clint, "Laboratory studies of electrical potential during rock failure," *International Journal of Rock Mechanics and Mining Sciences*, vol. 42, no. 7-8, pp. 933–949, 2005.

[27] Y. Zhao and Y. Jiang, "Acoustic emission and thermal infrared precursors associated with bump-prone coal failure," *International Journal of Coal Geology*, vol. 83, no. 1, pp. 11–20, 2010.

[28] X.-C. Xiao, X. Ding, and Y.-S. Pan, "Experiment of acoustic emission and charge induction in granular coal rock failure," *Journal of China Coal Society*, vol. 40, no. 8, pp. 1796–1804, 2015, Chinese in English Abstract.

[29] J. W. Archer, M. R. Dobbs, A. Aydin, H. J. Reeves, and R. J. Prance, "Measurement and correlation of acoustic emissions and pressure stimulated voltages in rock using an electric potential sensor," *International Journal of Rock Mechanics and Mining Sciences*, vol. 89, pp. 26–33, 2016.

[30] E. D. Pasiou and D. Triantis, "Correlation between the electric and acoustic signals emitted during compression of brittle materials," *Frattura ed Integrità Strutturale*, vol. 11, no. 40, pp. 41–51, 2017.

[31] M. Cai, P. K. Kaiser, Y. Tasaka, T. Maejima, H. Morioka, and M. Minami, "Generalized crack initiation and crack damage stress thresholds of brittle rock masses near underground excavations," *International Journal of Rock Mechanics and Mining Sciences*, vol. 41, no. 5, pp. 833–847, 2004.

[32] J. Lemaitre and J. L. Chaboche, *Mechanics of Solid Materials*, Cambridge University Press, Cambridge, UK, 1990.

[33] Z. X. Li, *Damage Mechanics and Its Application*, Science Press, Beijing, China, 2002.

[34] M.-Q. You and A.-Z. Hua, "Freacture of rock specimen and decrement of bearing capacity in uniaxial compression," *Chinese Journal of Rock Mechanics and Engineering*, vol. 17, no. 3, pp. 292–296, 1998, Chinese in English Abstract.

[35] R. Budakian and S. J. Putterman, "Correlation between charge transfer and stick-slip friction at a metal-insulator interface," *Physical Review Letters*, vol. 85, no. 5, pp. 1000–1003, 2000.

[36] X. Ding, X.-C. Xiao, D. Wu, and X.-F. Lv, "Mechanical properties and charge signal characteristics in coal material failure under different loading paths," *International Journal of Coal Science & Technology*, vol. 6, no. 1, pp. 138–149, 2019.

[37] X. Ding, X.-C. Xiao, X.-F. Lv, D. Wu, and Y. Pan, "Investigation on charge signal time-frequency domain characteristics in coal failure process and noise reduction," *Journal of China Coal Society*, vol. 43, no. 3, pp. 657–666, 2018.

[38] E.-Y. Wang, X.-Q. He, Z. T. Liu et al., "Study on frequency spectrum characteristics of acoustic emission in coal or rock deformation and fracture," *Journal of China Coal Society*, vol. 29, no. 3, pp. 289–292, 2004, Chinese in English Abstract.

[39] G.-S. Su, Y.-J. Shi, and X.-T. Feng, "Acoustic signal characteristics in rock-burst process," *Chinese Journal of Rock Mechanics and Engineering*, vol. 35, no. 6, pp. 1190–1201, 2016, Chinese in English Abstract.

[40] F. Vallianatos and D. Triantis, "Scaling in pressure stimulated currents related with rock fracture," *Physica A: Statistical Mechanics and its Applications*, vol. 387, no. 19-20, pp. 4940–4946, 2008.

[41] I. Stavrakas, C. Anastasiadis, D. Triantis, and F. Vallianatos, "Piezo stimulated currents in marble samples: precursory and concurrent-with-failure signals," *Natural Hazards and Earth System Science*, vol. 3, no. 3/4, pp. 243–247, 2003.